© 2015. Published by The Company of Biologists Ltd | Journal of Cell Science (2015) 128, 1365–1374 doi:10.1242/jcs.161414

RESEARCH ARTICLE

Impaired maturation of large dense-core vesicles in muted-deficient adrenal chromaffin cells

Zhenhua Hao[1,2], Lisi Wei[3], Yaqin Feng[1,4], Xiaowei Chen[3], Wen Du[5], Jing Ma[1], Zhuan Zhou[3], Liangyi Chen[3] and Wei Li[1,6,*]

ABSTRACT

The large dense-core vesicle (LDCV), a type of lysosome-related organelle, is involved in the secretion of hormones and neuropeptides in specialized secretory cells. The granin family is a driving force in LDCV biogenesis, but the machinery for granin sorting to this biogenesis pathway is largely unknown. The *mu* mutant mouse, which carries a spontaneous null mutation on the *Muted* gene (also known as *Bloc1s5*), which encodes a subunit of the biogenesis of lysosome-related organelles complex-1 (BLOC-1), is a mouse model of Hermansky–Pudlak syndrome. Here, we found that LDCVs were enlarged in *mu* adrenal chromaffin cells. Chromogranin A (CgA, also known as CHGA) was increased in *mu* adrenals and muted-knockdown cells. The increased CgA in *mu* mice was likely due a failure to export this molecule out of immature LDCVs, which impairs LDCV maturation and docking. In *mu* chromaffin cells, the size of readily releasable pool and the vesicle release frequency were reduced. Our studies suggest that the muted protein is involved in the selective export of CgA during the biogenesis of LDCVs.

KEY WORDS: Large dense core vesicle, BLOC-1, Muted protein, CgA, Hermansky–Pudlak syndrome

INTRODUCTION

Large dense-core vesicles (LDCVs), which are formed at the trans-Golgi network (TGN), are key organelles for secretion of hormones and neuropeptides in specialized secretory cells, including neuroendocrine and non-neuroendocrine cells. LDCVs are characterized as a type of lysosome-related organelle (LRO) (Wei and Li, 2013). However, the molecular players and mechanisms governing the biogenesis of LDCVs are not fully understood. During LDCV biogenesis, sorting machineries are important to ensure proper cargo assembly into mature and condensed vesicles (Kim et al., 2006; Tooze et al., 2001). Two hypotheses have been proposed for cargo sorting into LDCVs: sorting for entry and sorting for retention (Arvan and Castle, 1998). Prevention of cargo mis-sorting into lysosomes for degradation is also important during LDCV biogenesis (Yu et al., 2011).

[1]State Key Laboratory of Molecular Developmental Biology, Institute of Genetics & Developmental Biology, Chinese Academy of Sciences, Beijing 100101, China. [2]University of Chinese Academy of Sciences, Beijing 100039, China. [3]Institute of Molecular Medicine and State Key Laboratory of Biomembrane Engineering, Peking University, Beijing 100871, China. [4]Department of Histology and Embryology, Shanxi Medical University, Taiyuan 030001, China. [5]Institute of Biophysics, Chinese Academy of Sciences, Beijing 100101, China. [6]Center of Alzheimer's Disease, Beijing Institute for Brain Disorders, Beijing 100053, China.

*Author for correspondence (wli@genetics.ac.cn)

Received 6 August 2014; Accepted 2 February 2015

Previous studies have suggested that the granin family plays an important role in LDCV biogenesis (Kim et al., 2001), but the machinery for granin sorting into LDCVs is largely unknown. The adaptor protein-3 (AP-3) complex is likely involved in granin sorting into immature LDCVs. In AP-3-deficient chromaffin cells, LDCVs contain less granins, chromogranin A (CgA, also known as CHGA) and secretogranin II (SgII, also known as SCG2), and exhibit enlarged size, decreased number and an increase in releasing quantal size (i.e. the amount of transmitter released per vesicle) (Asensio et al., 2010; Grabner et al., 2006). AP-3 and the HOPS complex interact physically and might act in the same pathway in regulating endosomal trafficking (Angers and Merz, 2009; Rehling et al., 1999; Wilkin et al., 2008). Knockdown of VPS41 (a HOPS subunit) in PC12 cells leads to similar defects of LDCVs as in AP-3-deficient cells (Asensio et al., 2013). Similarly, the LDCVs in adrenal chromaffin cells from mice deficient in dysbindin [a subunit of biogenesis of lysosome-related organelles complex-1 (BLOC-1)] are reduced in number and increased in vesicle size, leading to reduced secretion events and increased quantal size (Chen et al., 2008). These findings suggest that AP-3, HOPS and BLOC-1 are likely involved in the sorting of cargoes into immature LDCVs (selective import) or the sorting of unnecessary molecules out of immature LDCVs (selective export). However, the underlying mechanisms of how these trafficking complexes control the import and export processes of LDCV proteins are very limited.

The BLOC-1 complex consists of eight subunits: muted, pallidin, dysbindin, cappuccino (also known as BLOC1S5, BLOC1S6, DTNBP1 and BLOC1S4, respectively), snapin, BLOS1 (also known as BLOC1S1 or GCN5L1), BLOS2 (also known as BLOC1S2) and BLOS3 (also known as BLOC1S3) (Ciciotte et al., 2003; Falcón-Pérez et al., 2002; Gwynn et al., 2004; Li et al., 2003; Starcevic and Dell'Angelica, 2004). KXD1 has been identified as an additional subunit of BLOC-1 (Hayes et al., 2011; John Peter et al., 2013; Yang et al., 2012). Current understanding of the functions of BLOC-1 are mainly focused on cargo trafficking from endosomes to lysosomes (for a review, see Wei and Li, 2013) and endosomal maturation (John Peter et al., 2013). BLOC-1 deficiency causes Hermansky–Pudlak syndrome (HPS) in mice and humans, which is characterized by LRO dysfunction (Wei and Li, 2013). The KXD1-knockout mice (Yang et al., 2012) exhibit mild defects in LROs compared with other typical HPS mouse mutants of BLOC-1 such as the *sdy* (dysbindin deficiency), *mu* (muted deficiency) and *pa* (pallidin deficiency) mice, whereas snapin- and BLOS1-knockout mice are embryonic lethal and exhibit impaired autophagy (Cai et al., 2010; Scott et al., 2014; Tian et al., 2005; Zhang et al., 2014). This suggests that the deficiency of different BLOC-1 subunit leads to variable phenotypes on LROs. Comparison of the

Journal of Cell Science (2015) 128, 1365–1374 doi:10.1242/jcs.161414

features of LRO defects in different BLOC-1 mouse mutants might reveal the underlying mechanisms in their involvement of LRO biogenesis.

The *mu* mutant mouse, which carries a spontaneous mutation on the *Muted* gene (*Bloc1s5*), abolishes the expression of the muted protein and affects the biogenesis of several LROs such as melanosomes and platelet-dense granules (Zhang et al., 2002). In our pilot study, we observed that *mu* mice had a different profile of morphological changes in LDCVs compared to *sdy* mice (Chen et al., 2008) or snapin-knockout mice (Pan et al., 2009; Tian et al., 2005). In comparison with additional HPS mouse mutants, we propose that the muted protein is involved in the export of the granin CgA during LDCV biogenesis.

RESULTS

Morphological changes of LDCVs in *mu* chromaffin cells

To investigate whether LDCVs are affected in *mu* mice (*mu/mu*), we analyzed the morphological changes of LDCVs from adrenal gland of controls (*mu*/+) and *mu* mice by electron microscopy. The gross ultrastructure of *mu* chromaffin cells was similar to that in the control mice (Fig. 1A). The round granular limits were visible and dense cores were condensed in *mu* chromaffin cells. In control cells, many granules had a loosely packaged dense-core and a spacious halo around the dense core. However, in *mu* cells, the halos were less spacious and the dense cores occupied more of the space in the whole vesicles (Fig. 1A). We then examined the number and size of LDCVs in sections of randomly selected cells from two different animals for each genotype. There was no significant difference in the total number of vesicles per square micrometer between control and *mu* chromaffin cells (Fig. 1B). For vesicle size analysis, all round granules with a well-preserved membrane, a halo and an electron-dense round core were included. The average increase of the size (diameter) of LDCVs in *mu* chromaffin cells was ~6% (Fig. 1C). Furthermore, the electron-dense core size (diameter) was significantly enlarged by ~17.6% in *mu* chromaffin cells (Fig. 1D). Hence, the ratio of dense core diameter compared to vesicle diameter was increased by ~10% in *mu* mice compared with control mice (Fig. 1E). Similarly, we observed enlarged vesicle size and dense core size in another type of LDCV in islet α-cells, which contain CgA and glucagon (Portela-Gomes and Stridsberg, 2001), in the *mu* mice (supplementary material Fig. S1). These results suggest that loss of the muted protein likely affects LDCV morphology in a conserved mechanism.

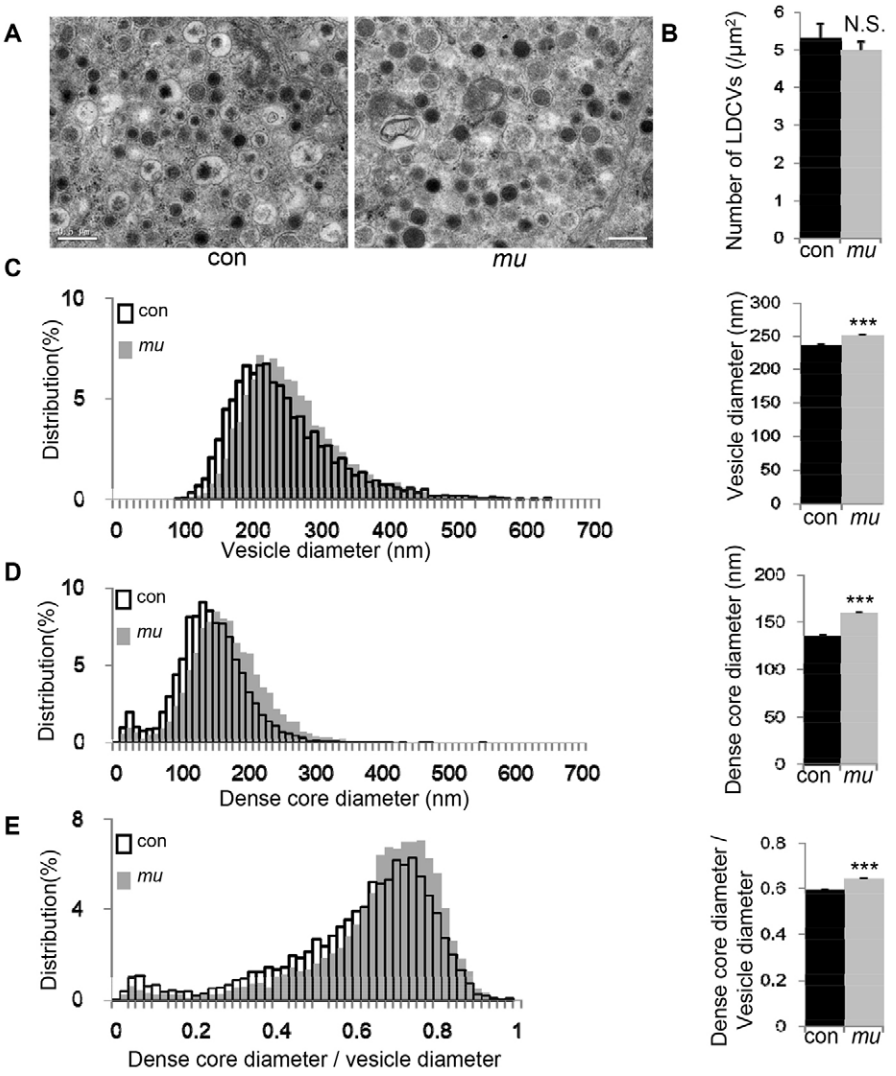

Fig. 1. Ultrastructural pathology of LDCVs in *mu* chromaffin cells. (A) Representative electron micrographs of adrenal gland sections from heterozygous *mu*/+ (con, left) and homozygous *mu/mu* (*mu*, right) male mice at the age of 8 weeks. Scale bars: 0.5 μm. (B) There was no significant difference in the total number of vesicles in *mu* mice (con: 5.34±0.36 vesicles/μm^2; *mu*: 5.00±0.24 vesicles/μm^2). Results are mean±s.e.m. N.S., not significant. (C) The LDCV diameter is presented as a frequency histogram. The mean diameter of the LDCVs increased in *mu* mice (251.25±0.88 nm, 6244 vesicles) compared with that in control mice (237.30±0.87 nm, 7664 vesicles). ***P<0.001. (D) The electron-dense core diameter is presented as a frequency histogram. The average diameter of electron-dense cores increased in *mu* mice (159.43±0.71 nm, 6244 vesicles) compared with that in control mice (135.52±0.60 nm, 7664 vesicles). ***P<0.001. (E) The dense core diameter/LDCV diameter is presented as a frequency histogram. The ratio of dense core diameter:vesicle diameter was higher in *mu* mice (0.645±0.002, 6244 vesicles) than in control mice (0.594±0.002, 7664 vesicles). ***P<0.001.

Journal of Cell Science (2015) 128, 1365–1374 doi:10.1242/jcs.161414

Muted deficiency increases the amount of CgA in LDCVs in adrenal glands and PC12 cells

CgA is a major constituent of LDCVs, acting as an assembly factor to drive secretory granule biogenesis (Kim et al., 2001). To investigate the molecular mechanism of the morphological defects of *mu* LDCVs, we measured the steady-state protein levels of CgA in adrenal glands in *mu* mice. We found a significant increase (1.54-fold) of full-length CgA (80 kDa) in *mu* mice compared to wild-type (WT, con) mice (Fig. 2A,B). We quantified the amount of an intermediate CgA-derived peptide (~23 kDa) and there was likewise an increase in *mu* mice (Fig. 2C,D), which is in agreement with the increase of full-length CgA. This suggests that the increased CgA in *mu* mice is unlikely to be caused by the inefficiency of CgA cleavage. In contrast, the protein levels of another granin, SgII, were unaltered in *mu* mice compared to control mice (Fig. 2E,F). We confirmed the increase of CgA in muted-knockdown (KD) PC12 cells (Fig. 2G). Consistently, the intensities of CgA in muted-KD PC12 cells was significantly increased (Fig. 2H,I).

As the total number of LDCVs in *mu* cells did not change, we reasoned that the increased CgA might result from impaired export from immature LDCVs or from mislocalized non-LDCV organelles. We monitored the distribution of CgA by western blotting after equilibrium sedimentation through a 5–50% OptiPrep gradient. We found an almost complete absence of CgA of *mu* adrenal glands in the lighter fractions 3 and 4, which correspond to the clathrin heavy chain, compared with in wild-type mice. In contrast, the distribution of SgII was similar between *mu* and WT mice (Fig. 3A). These results suggest that the muted protein might facilitate the removal or export of CgA from immature secretory granules (ISGs) via clathrin-coated vesicles (Orci et al., 1985a; Tooze and Tooze, 1986).

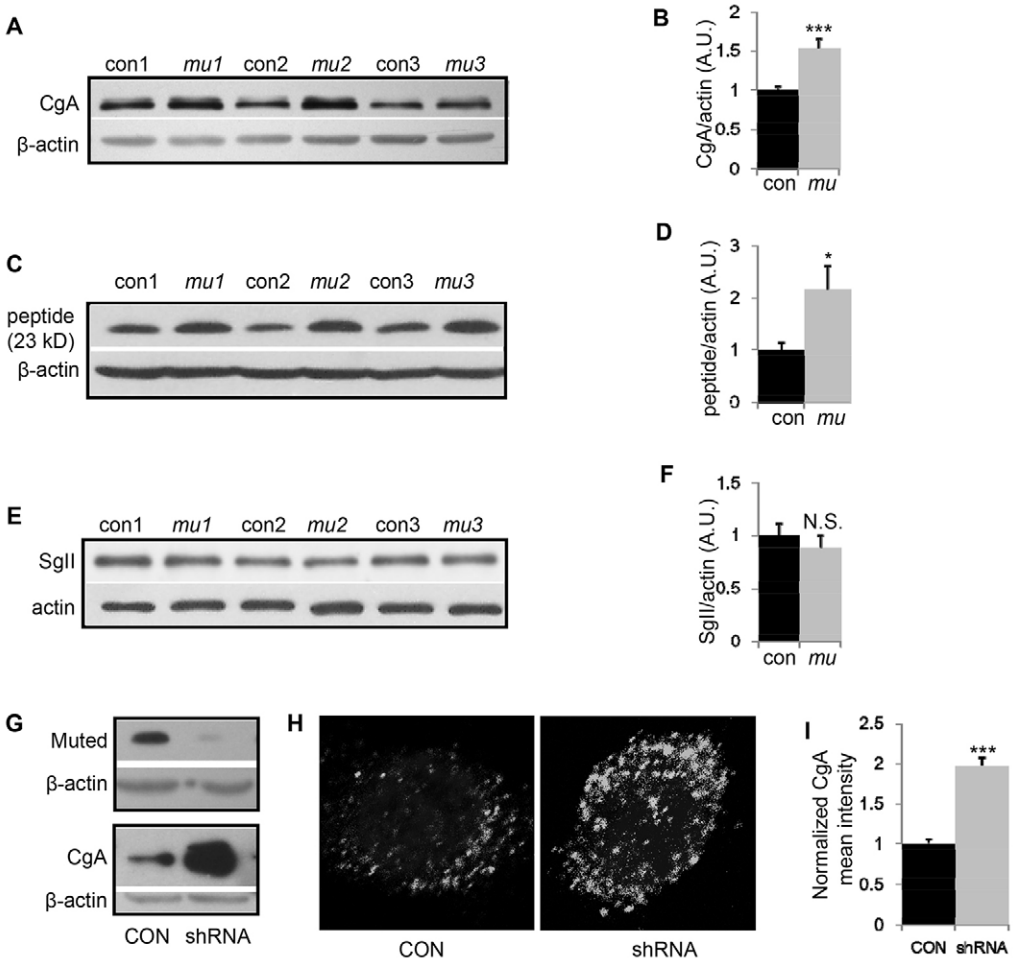

Fig. 2. Increased CgA levels in *mu* adrenal glands and muted-knockdown cells. (A,B) Representative western blots of CgA are shown. Quantification of the immunoblotting analyses showed that there was an increase in full-length CgA in adrenal glands of *mu* mice (n=28) relative to wild-type (con) mice (n=28). ***P<0.001. (C,D) Representative western blots of CgA-derived peptide (~23 kDa) are shown. Quantification of immunoblotting analyses showed that there was an increase in CgA-derived peptide in adrenal glands of *mu* mice (n=8) compared to control mice (n=8). *P<0.05. (E,F) Representative western blots of SgII are shown. Quantification of immunoblotting analyses showed that there was no significant change in SgII levels in adrenal glands of *mu* mice (n=8) compared to control mice (n=9). N.S., not significant. (G) Immunoblotting analyses of lysates from stable muted-shRNA PC12 cells (shRNA) showed an ~90% reduction of muted protein relative to control cells (CON) (upper panel). Cellular CgA was drastically increased in muted-shRNA PC12 cells compared to control cells as shown by immunoblotting (lower panel). The immunoblots shown are representative of at least three independent experiments. (H) Representative immunofluorescence images of CgA in muted-shRNA PC12 cells and control cells. (I) Average fluorescence intensities of CgA were increased in muted-shRNA PC12 cells. Fluorescence intensities of CgA were quantified from 63 muted-shRNA PC12 cells and 57 control cells, respectively. ***P<0.001. Results in B, D, E and I are mean±s.e.m.

Journal of Cell Science

Journal of Cell Science (2015) 128, 1365–1374 doi:10.1242/jcs.161414

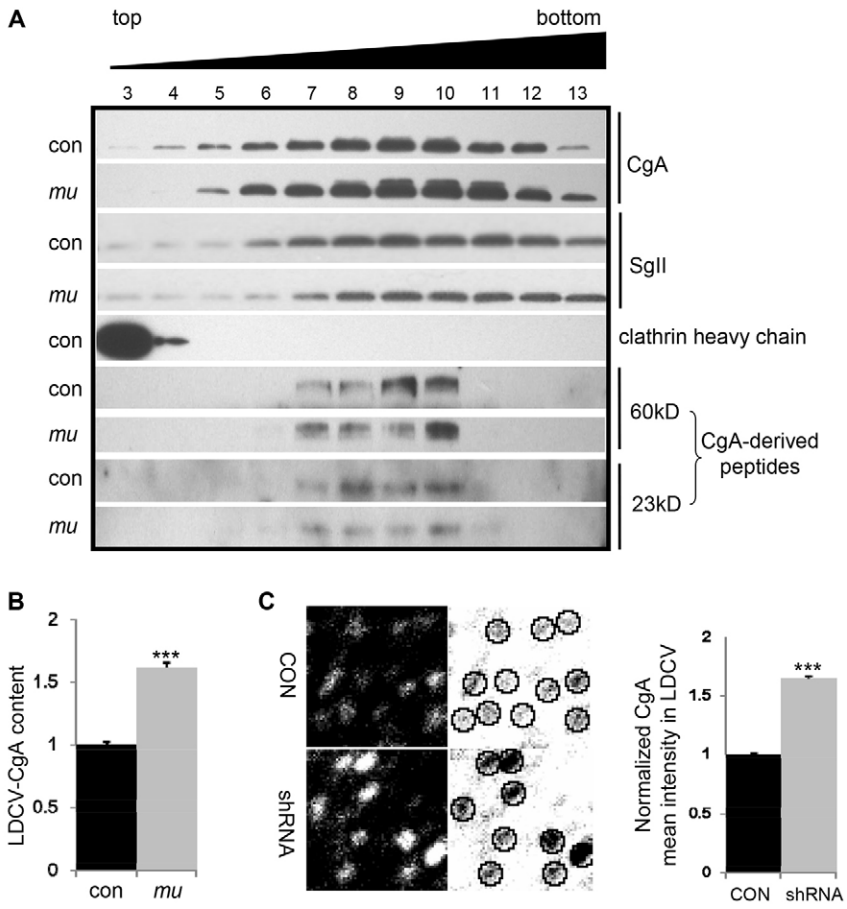

Fig. 3. Increased CgA levels in *mu* LDCVs. (A) Adrenal glands from wild-type (con) and *mu* mice were homogenized and the nuclei-free supernatant was separated by equilibrium sedimentation through 5–50% Optiprep. Fourteen fractions were collected from the top of the gradient and assayed for CgA by immunoblotting; 11 fractions are shown on the blots. Note that CgA was almost completely absent from fractions corresponding to the clathrin heavy chain in *mu* lysates as compared to the distribution of SgII in the same lysates, which did not show any difference to that in control lysates. CgA-derived peptides (60 kDa and 23 kDa) were enriched in fractions 7–10, which represent the LDCV peak. (B) Quantification of nine western blots from three independent sedimentations showed that the amount of CgA (80 kDa) in the LDCV peak was increased in lysates from *mu* mice (1.61±0.04) compared with those from control mice (1.00±0.02). ***$P<0.001$. Results are mean±s.e.m. CgA content in LDCV peak is expressed as a percentage of total CgA normalized to the control group and total CgA. The percentage for the LDCV peak in the sedimentations was multiplied by a factor of 1 for the control group, and by a factor of 1.54 for the *mu* group because the average amount of total CgA in the *mu* group is 1.54-fold that of the control group (shown in Fig. 2B). (C) The mean fluorescence intensity of CgA of individual cytosolic vesicles, as shown in the left panel, in muted-knockdown PC12 cells was significantly increased (1.65±0.02, $n=4879$ vesicles) compared to the control cells (1.00±0.01, $n=4694$ vesicles). Individual vesicles were selected in 10×10 pixels regions (1 pixel=62 nm) and the CgA fluorescence of each vesicle was measured. *** $P<0.001$. Results are mean±s.e.m.

We then tested whether the increased amount of CgA in *mu* mice was localized to LDCVs or mislocalized to other organelles. Immature and mature LDCVs have been considered as the major prohormone conversion sites (Koshimizu et al., 2010; Orci et al., 1985b). In this regard, the processed CgA peptides (60 kDa and 23 kDa) are mainly concentrated in LDCVs. We observed that these peptides were enriched in fractions 7–10, which represent the distribution of LDCVs (Fig. 3A). We then quantified the total amount of CgA in these LDCV-enriched fractions and our results showed that the LDCV-CgA proportion in *mu* mice was increased compared with the WT mice (Fig. 3B). Consistent with this, we quantified the intensities of CgA in cytosolic individual granules that are defined as LDCVs (Walter et al., 2014) and showed that the CgA intensity in the LDCV proportion was increased in muted-KD PC12 cells compared with the control cells (Fig. 3C).

To confirm that loss of muted protein leads to the increase in CgA, we transfected EGFP–muted into the stable muted-knockdown PC12 cells (Fig. 4A). We quantified the intensities of total CgA and the CgA in individual LDCVs in the transfected cells and showed that both total CgA and the LDCV-CgA proportion were significantly decreased in the EGFP–muted-expressing cells compared with the EGFP-transfected cells (Fig. 4B,C). We verified the expression of the muted protein in these cells (Fig. 4D). These results suggest that the increased LDCV-CgA as well as total CgA can be rescued by the expression of functional muted protein.

We then investigated whether CgA is mislocalized to other non-LDCV organelles in the *mu* cells. We observed that CgA was largely retained in the SgII-positive LDCVs in both the muted-KD cells and control cells, with a partial colocalization with LAMP1, which is a marker of both lysosomes and LDCVs. We did not observe apparent mislocalization of CgA to other organelles including the endoplasmic reticulum (ER) (SEC61B), TGN (STX6), early endosomes (EEA1) and late endosomes (Rab7) in the muted-KD cells when compared to control cells (Fig. 5), suggesting that its subcellular localization is unaltered.

Taken together, in the absence of muted protein, the proportion of CgA which is sorted to constitutive secretory vesicles or lysosomes might be trapped in ISGs, and thus lead to the increase of CgA in LDCVs. As CgA has the ability to aggregate to form electron-dense cores, the increased CgA content in *mu* chromaffin cells likely leads to the increased size of electron-dense cores as well as the increased size of LDCVs.

Loss of muted protein leads to a smaller readily releasable pool size and a reduction in vesicle secretion

We tested whether the size change in LDCV in *mu* cells would affect the size of the readily releasable pool (RRP) and the release frequency. In neuroendocrine cells, the RRP generally represents the population of fusion-competent vesicles, and the immediately releasable pool (IRP) corresponds to a subpool of the RRP that is closely associated with Ca^{2+} channels (Voets et al., 1999). Whole-cell patch-clamp was applied to single chromaffin cells. Average responses obtained from control and *mu* mice showed that secretory response was drastically reduced in *mu* chromaffin cells as shown by the reduced IRP and RRP size (Fig. 6A–D). These results indicate that lack of muted protein leads to a smaller RRP size and results in a reduction of vesicular secretion in chromaffin cells.

Journal of Cell Science (2015) 128, 1365–1374 doi:10.1242/jcs.161414

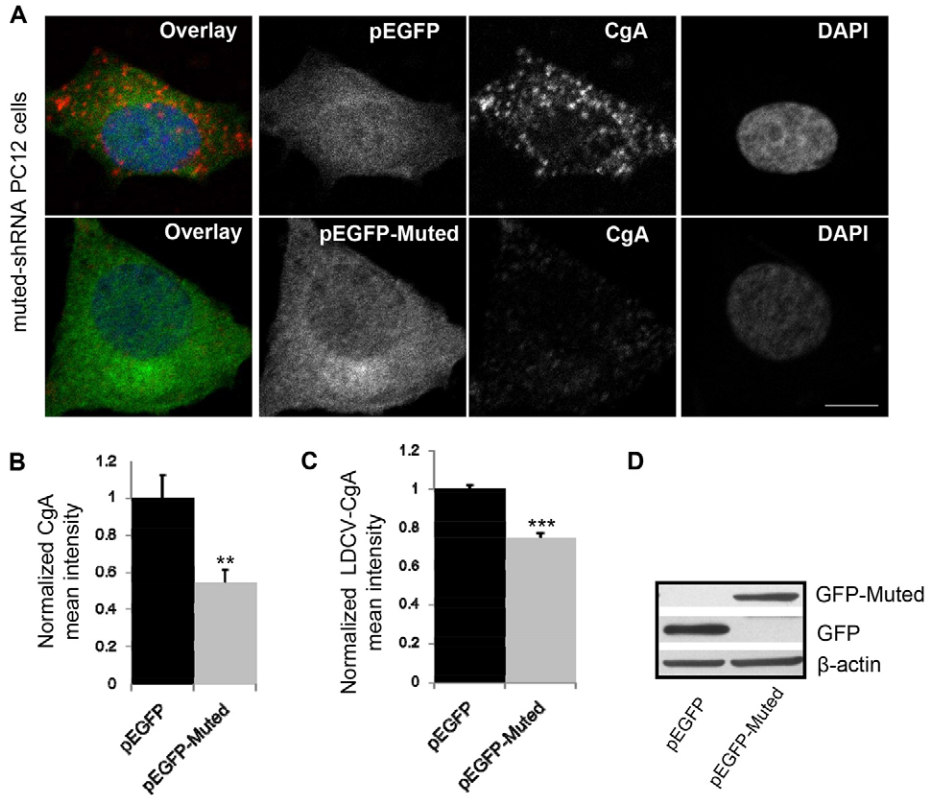

Fig. 4. Expression of muted protein in the muted-knockdown PC12 cells reduced the CgA content in the LDCVs. (A) Expression of full-length *Muted* cDNA in the muted-shRNA PC12 cells reduced the CgA content. Muted-shRNA PC12 cells were transfected with pEGFP-C2 or pEGFP-C2-Muted, to express an EGFP–Muted fusion protein, (green) for more than 72 hours and immunostained for CgA (red). Cells with EGFP green signals were counted. Scale bar: 5 μm. (B,C) Quantification of CgA fluorescence intensities showed that expression of EGFP–Muted reduced the total CgA level (control, 1.00±0.12, n=64 cells; Muted group, 0.54±0.07, n=64 cells.) and LDCV-CgA level (control, 1.00±0.02, n=2222 vesicles; Muted group, 0.75±0.02, n=1443 vesicles;) in *mu* chromaffin cells. $^{**}P<0.01$, $^{***}P<0.001$. (D) Immunoblotting showing that EGFP–Muted-transfected cells express muted protein.

The reduction in RRP size or vesicle release could result from the reduction of docked vesicles when LDCV maturation is impaired, as evident by the enlargement of LDCVs in *mu* cells. We measured the number of docked vesicles (0–100 nm from plasma membrane) in the *mu* adrenal chromaffin cells. Indeed, the docked vesicles in *mu* cells were significantly reduced compared to the control mice (Fig. 6E,F).

We then investigated that whether the docked vesicles release with normal kinetics. We recorded the kinetics of each releasing spike by carbon-fiber electrodes. We found no significant changes in half-height duration (HHD), rise time (RT) and quantal size (Q) of amperometric spikes between control and *mu* mice (supplementary material Fig. S2). This suggests that the docked vesicles might represent a normal population of LDCVs that have normal fusion and release kinetics. This population might not be affected by the muted protein.

To explore whether the docking or fusion machinery is affected by the loss of muted protein, we determined the steady state levels of the synaptic proteins in the *mu* adrenal glands. Western blotting analyses confirmed the expression of the muted protein in adrenal cells. As expected, no band was observed in the *mu* adrenal glands. We did not find apparent changes in the steady-state levels of a panel of synaptic proteins including SNARE proteins (SNAP25, syntaxin-1 and VAMP2), synaptophysin (SYP) and Munc18 between controls and *mu* mice (supplementary material Fig. S3A). These results suggest that the smaller RRP pool does not result from changes in the steady-state levels of these well-known docking or fusion proteins.

Muted protein affects the steady-state CgA levels in adrenal glands differently from other proteins known to affect LDCVs

Compared with the characteristics of LDCVs in dysbindin-1 deficient *sdy* mice, *mu* mice have a different profile of LDCV phenotypes (supplementary material Table S1) although both dysbindin-1 and muted reside in the same BLOC-1 complex. This suggests that dysbindin-1 and muted play different roles in cargo sorting for LDCV biogenesis. Notably, vesicle number is reduced in *sdy* mice but is normal in *mu* mice. The reduction of LDCV number in AP-3- or HOPS-deficient chromaffin cells might lead to the decrease of CgA and SgII as shown in supplementary material Table S1. We confirmed the reduction of CgA and SgII in *pe* (β3A AP-3 deficiency) and *bf* (VPS33a HOPS deficiency) mice compared with their wild-type controls. In *sdy* mice, CgA was decreased and that there was also a reduction in the levels of SgII although this was not significant (Fig. 7). In contrast, the CgA steady-state level was increased but SgII was normal and the number of LDCVs was not changed in *mu* mice (Figs 1, 2). This suggests that the increase in CgA in *mu* mice is not due to the increase in LDCV number. This further supports our hypothesis that the increase of CgA in *mu* cells is caused by the retention of CgA in immature LDCVs. Muted protein plays an important role in the export of CgA, but has no or little effect on SgII.

DISCUSSION

Here, we characterized the defects in LDCV morphology (enlarged size and reduced docking) by examining electron microscopy images of *mu* adrenal chromaffin cells. In the absence of muted protein, the CgA content was increased, which could be an explanation for the enlarged sizes of LDCVs and dense cores (Kim et al., 2001). The increase of CgA does not result from an increased vesicle number or impaired processing, rather it is likely caused by the failure of CgA export from the vesicles when muted protein is lacking. In general, an enlarged size of LDCV represents immature LDCVs (Kim et al., 2006). Consequently, failure of CgA export might impair LDCV maturation and docking and finally vesicle release (supplementary material Fig.

Journal of Cell Science (2015) 128, 1365–1374 doi:10.1242/jcs.161414

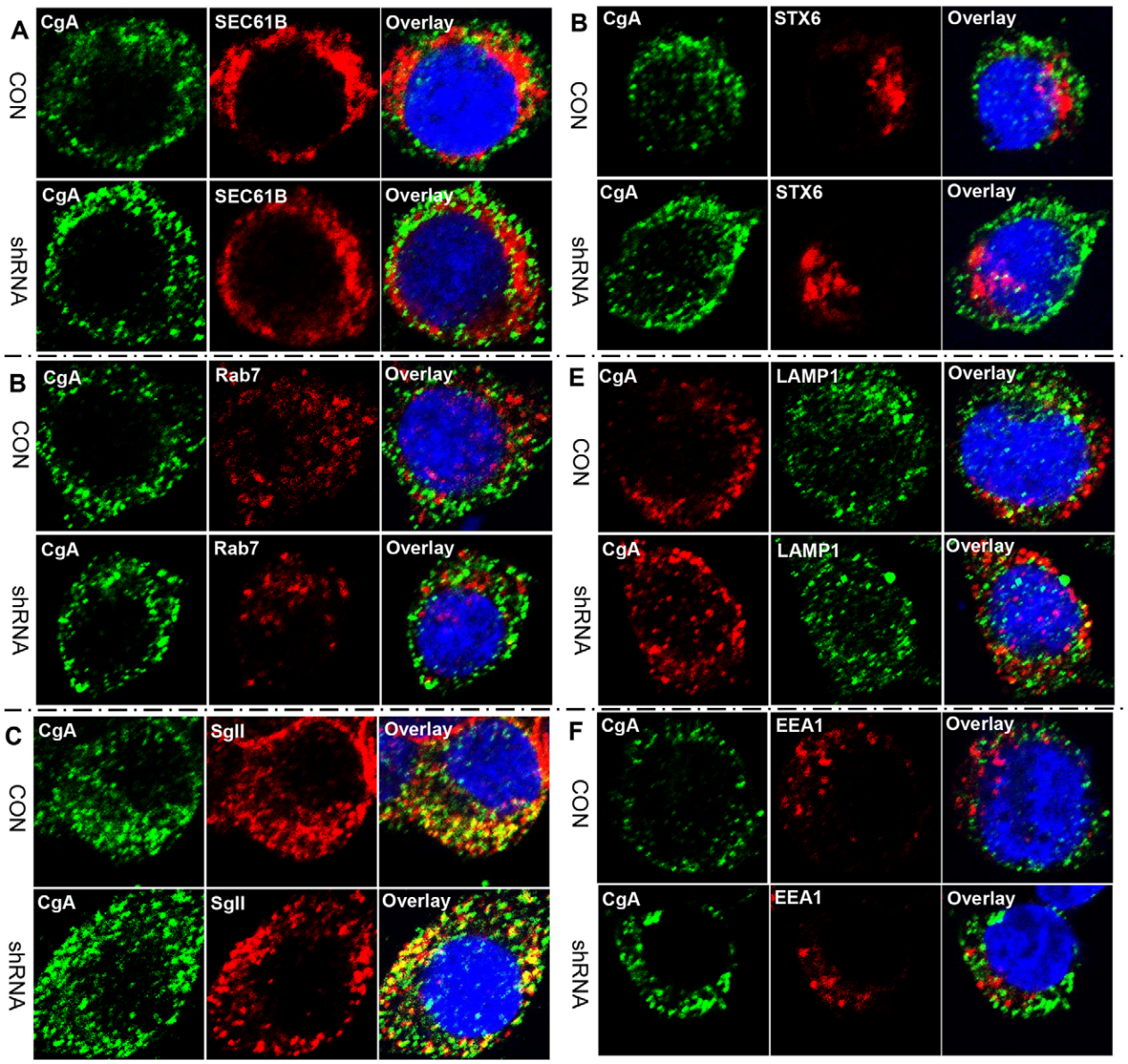

Fig. 5. Subcellular localization of CgA in muted-shRNA PC12 cells. Representative images of subcellular localization of CgA in control (CON) and muted-shRNA (shRNA) PC12 cells. CgA was detected by co-immunostaining with CgA and different organelle markers, [the ER marker SEC61B (A), the multivesicular body marker Rab7 (B), the LDCV marker SgII (C), the TGN marker STX6 (D), the lysosome marker LAMP1 (E), and the early endosome marker EEA1 (F)]. Note that the intensities of CgA were increased in shRNA cells, and that CgA was mainly retained in the LDCVs in shRNA cells rather being than mislocalized to other organelles.

S3B). These findings support the sorting-for-retention model and provide molecular insights into the sorting machinery of LDCV and its pathology.

Cargo sorting into LDCVs is a very complicated and highly regulated process. It has been postulated that there different LDCV populations exist, which might have different constituents (Duncan et al., 2003; Grabner et al., 2005; Watanabe et al., 1991). The segregation of CgA and SgII in different populations implicates that there exist different sorting machineries for these granins (Watanabe et al., 1991). As shown in Fig. 5C, there were some granules that CgA and SgII did not colocalize in control cells, further supporting that separate CgA-positive vesicles and SgII-positive vesicles exist, although a large number of the granules contain both CgA and SgII. Furthermore, our results showed an increase in CgA but a normal level of SgII, and a distributional shift in CgA, but not SgII, in the *mu* adrenal glands. This indicates that the muted protein is involved in the sorting of CgA, but not SgII. This also explains why vesicle docking and release events exist and why the releasing kinetics is normal (supplementary material Fig. S2) in the *mu* chromaffin cells given that the secretion of SgII-positive LDCV population is normal.

Control of vesicle number and size could be a reflection of the complexity of multiple regulators. In BLOC-1, loss of dysbindin-1 (*sdy*) and loss of muted (*mu*) both lead to an enlargement of LDCV size, but the LDCV number is unchanged in *mu* mice, in contrast to reduced LDCV numbers in *sdy* mice (Chen et al., 2008). In other LROs, such as melanosomes and platelet-dense granules, both *mu* and *sdy* mice show reduced vesicle numbers,

Journal of Cell Science (2015) 128, 1365–1374 doi:10.1242/jcs.161414

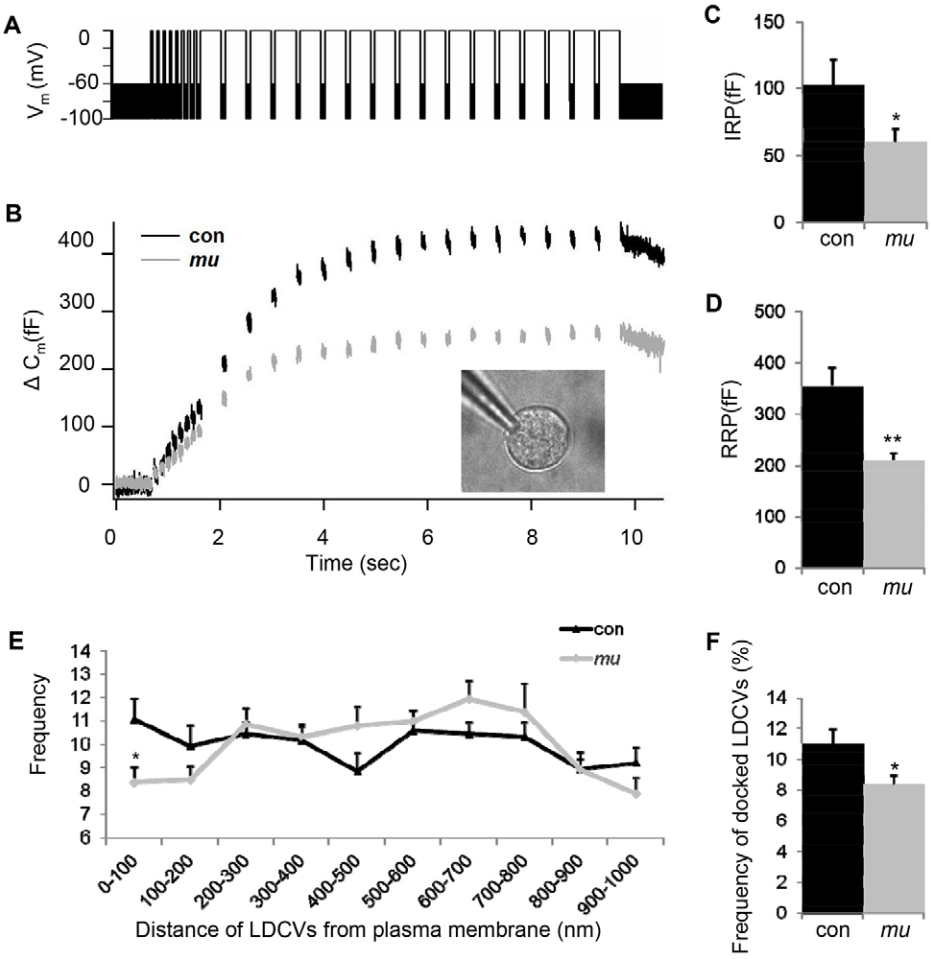

Fig. 6. Reduced depolarization-induced secretion and docked LDCVs in *mu* chromaffin cells. (A) A schematic showing the trains of eight 50-ms depolarizations from −80 to 0 mV with a 100-ms interpulse interval were used to estimate the IRP size, followed by seventeen 500-ms depolarizations to estimate the RRP size. (B) Average capacitance increase of control (19 cells from four *mu*/+ mice, black) and *mu* (22 cells from four *mu*/*mu* mice, grey) chromaffin cells in response to trains of depolarizing pulses. (C,D) The averaged values of the IRP (C) and RRP (D) showed a great reduction in *mu* cells compared with control. The IRP size of each single chromaffin cell was determined as the maximum capacitance responses (ΔCm) during the eight ~10-ms depolarizations, whereas the RRP size was determined as the maximum capacitance responses during the seventeen ~500-ms period. Note that the RRP includes the IRP. In control chromaffin cells, we observed an average size of 102.38±19.23 fF for the IRP (n=19) and 354.84±35.19 fF (n=19) for the RRP. In *mu* chromaffin cells, the IRP size was reduced by ~40% (60.04±9.97 fF; n=22; *P<0.05), and the RRP size was reduced by ~40% (209.92±15.13 fF; n=22; **P<0.01). (E) Distribution of distance between vesicle membrane and plasma membrane in *mu* mice (*mu*/*mu*) and control mice (*mu*/+). (F) Vesicles located within 100 nm from the plasma membrane were defined as morphologically docked vesicles and counted. There was a lower frequency of morphologically docked LDCVs in *mu* (8.38±0.65%, n=1 565 vesicles from 10 cells of two *mu*/*mu* mice) cells than that in controls (11.05±0.91%, n=2 054 vesicles from 12 cells of two *mu*/+ cells). *P<0.05. Results are mean±s.e.m.

indicating the biogenesis of LROs utilizes shared mechanisms in endo-lysosomal trafficking (Swank et al., 1998; Wei and Li, 2013). Taken together, mounting evidence indicates that each LRO has unique biosynthetic and cargo-sorting pathways, although they might share some common sorting mechanisms. By contrast, dysbindin is known to bind to a variety of proteins belonging to the dystrophin protein complex, the WAVE-2 complex and others (Ghiani and Dell'Angelica, 2011; Li et al., 2007). This suggests that different interacting partners of BLOC-1 subunits are operative (Li et al., 2007). In addition, dysbindin-1 has distinct isoforms that might function in different pathways (Talbot et al., 2009). We have recently shown that dysbindin-1C isoform functions in a BLOC-1-independent pathway in regulating autophagy and neuronal survival (Wang et al., 2014; Yuan et al., 2015). The altered ultrastructure of hippocampal synaptic vesicles might cause reduced neurotransmission and thereafter the schizophrenia-like symptoms observed in *sdy* mice (Chen et al., 2008; Feng et al., 2008; Wang et al., 2014). However, except for *DTNBP1* and *BLOC1S3*, genes encoding other BLOC-1 subunits have no significant association with schizophrenia although an epistatic interaction between *DTNBP1* and *MUTED* might exist (Morris et al., 2008). Currently, there is no support for *MUTED* as a susceptibility gene for schizophrenia (Gerrish et al., 2009). Thus, the different profiles of releasing vesicle defects in *sdy* and *mu* mice might have different mechanisms and consequences.

CgA has been implicated in playing multiple roles in the endocrine, cardiovascular and nervous systems through the regulation of multiple DCV biogenesis in different tissues. Our results have shown similar defects in both the adrenal chromaffin LDCV and the LDCV in pancreatic islet α-cells (supplementary material Fig. S1), suggesting that they might share a conserved mechanism in CgA sorting. CgA knockout in mice leads to

Journal of Cell Science (2015) 128, 1365–1374 doi:10.1242/jcs.161414

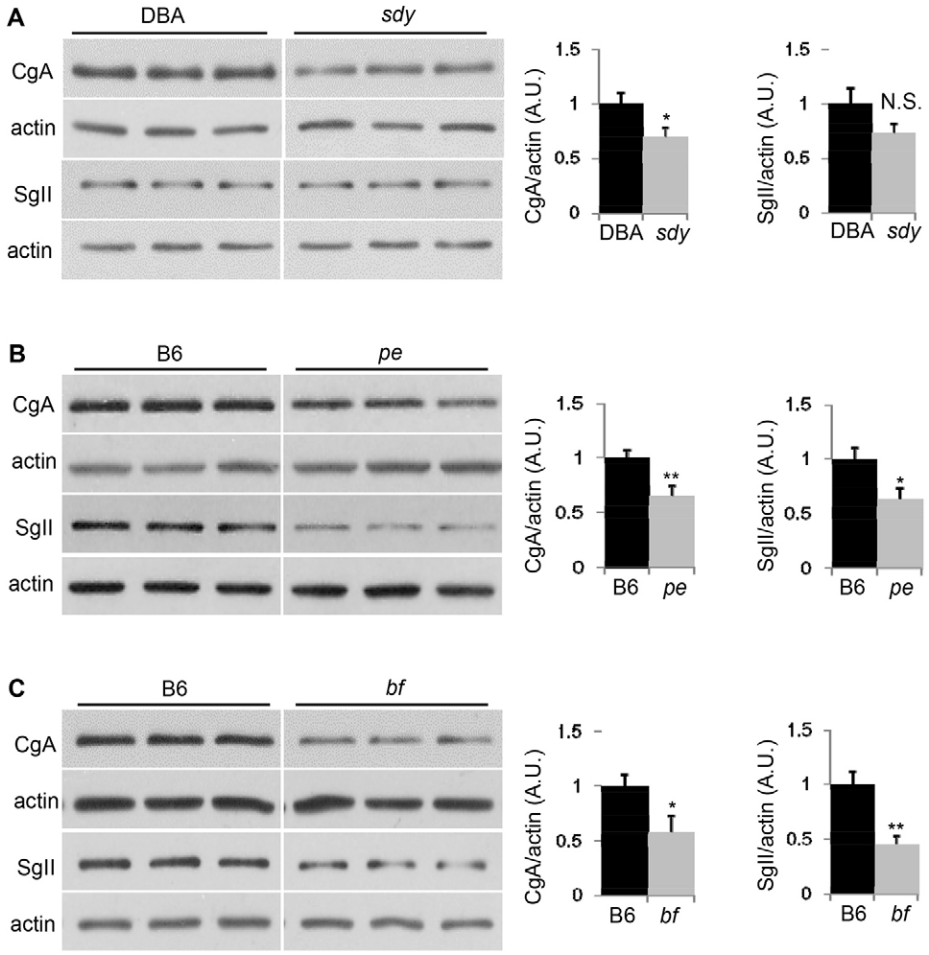

Fig. 7. The content of CgA and SgII in the adrenal glands of HPS mice. (A) Western blots of the protein levels of CgA and SgII in the adrenal glands of *sdy* mice (dysbindin BLOC-1 deficiency) and their control DBA/2J littermates. Quantitative analyses showed that there was a decrease in the amount of CgA (n=8, *P<0.05) and that there was also a reduction in the amount of SgII, although this was not significant (n=8, N.S., not significant) in *sdy* mice. (B) Western blots of the protein levels of CgA and SgII in the adrenal glands of *pe* mice (β3A AP-3 deficiency) and their control C57BL/6J (B6) littermates. Quantitative analyses showed a decrease in CgA (n=12, **P<0.01) and SgII (n=12, *P<0.05) in *pe* mice. (D) Western blots of the protein levels of CgA and SgII in adrenal glands of *bf* mice (VPS33a HOPS deficiency) and their control C57BL/6J (B6) littermates. Quantitative analyses showed a decrease in CgA (n=4, *P<0.05) and SgII (n=6, **P<0.01) in *bf* mice. Results are mean±s.e.m.

decreased size and number of LDCVs in chromaffin cells, as well as hypertension in these animals (Mahapatra et al., 2005). In our case, loss of muted protein causes an increase in CgA and impairs LDCV release frequency from the chromaffin cells. Whether CgA secretion is reduced *in vivo* in *mu* mice, or whether there is a link to hypertension or other LDCV phenotypes in this mutant requires further detailed investigation.

MATERIALS AND METHODS

Mice

The *mu* mutant mice and control CHMU/Le mice (wild-type, WT) were as described previously (Zhang et al., 2002). Other mouse mutants and their controls including pearl (*pe*) and buff (*bf*) in the C57BL/6J (B6) background, sandy (*sdy*) in the DBA/2J (DBA) background were are summarized Li et al. (Li et al., 2004). They were originally obtained from the Jackson Laboratory (Bar Harbor, Maine, USA), were transferred to Dr Richard T. Swank's laboratory at Roswell Park Cancer Institute (Buffalo, New York, USA) and are bred in the animal facility of the Institute of Genetics and Developmental Biology, Chinese Academy of Sciences. All animal experiments were performed under permission from the Institutional Animal Care and Use Committee and the Peking University Committee on Ethics in the Care and Use of Laboratory Animals. The genotypes of wild type (+/+), heterozygous (*mu*/+) and homozygous (*mu*/*mu*) mice were identified by a PCR method based on the mutation in the *Muted* gene (Zhang et al., 2002). Age-matched wild-type CHMU/Le mice and heterozygous mice were used as background controls.

Antibodies

The polyclonal muted antibody was generated in New Zealand white rabbits against a His-tagged fusion protein corresponding to the mouse full-length muted protein (GenBank RefSeq NM_139063). The mouse monoclonal antibodies against Syntaxin 6 (#ab12370), the rabbit polyclonal CgA (#ab45179), VAMP2 (#ab3347) and SEC61B (#ab78276) were obtained from Abcam (Cambridge, UK). The rabbit polyclonal Rab7 (#9367) and clathrin heavy chain (#4796) antibodies were from Cell Signaling Technology (Danvers, MA). The rabbit polyclonal SgII antibody (#K55101R) was from Meridian Life Science (Memphis, TN). The mouse monoclonal β-actin antibody (#A5441) was purchased from Sigma-Aldrich (St. Louis, MO). The mouse monoclonal EEA1 (#610457), Munc-18 (#610337) and the rat monoclonal LAMP1 (#553792) antibodies were from BD Biosciences (San Diego, CA). Mouse monoclonal SYP (#sc-17750), syntaxin 1 (#sc-12736), SNAP25 (#sc-20038), GFP (#sc-9996) and goat polyclonal CgA (#sc-1488) antibodies were purchased from Santa Cruz Biotechnology (Dallas, TX).

Immunoblotting

Adrenal glands from control and *mu* mice were homogenized in 50 mM Tris-HCl pH 7.4, 150 mM NaCl, 1% Triton X-100, and a protease inhibitor cocktail (Sigma-Aldrich). The extracts were centrifuged at 13,000 ***g*** for 15 min to remove nuclei and cell debris, equal amounts of homogenates were separated on 12% SDS-PAGE gels and transferred onto polyvinylidene difluoride (PVDF, Millipore) membranes. The membranes were immunoblotted with specific antibodies and visualized by ECL (Pierce, Rockford, IL). Protein bands intensities were quantified by NIH Image J after normalization to β-actin.

OptiPrep gradient assay

Adrenal glands from WT and *mu* mice were homogenized in 300 µl HB buffer (250 mM sucrose, 20 mM Tris-HCl, 1 mM EDTA, pH 7.4) plus a protein inhibitor cocktail (Sigma-Aldrich). A post-nuclear supernatant (PNS) was generated by centrifugation at 1000 ***g*** for 10 min. The PNS

was layered onto a linear 5–50% linear Optiprep gradient (Axis-Shield, Norway) formed in HB buffer using a Gradient Master (Biocomp, USA). Gradients were spun at 30,000 rpm for 15–16 hours in an SW41 rotor (Beckman, USA) at 4℃. Fourteen equal fractions (900 µl each) were collected from the top of the gradient and subjected to acetone precipitation. The precipitated protein (fractions 3–13) was analyzed by SDS-PAGE and immunoblotting.

Cell culture and transfections

PC12 cells were cultured at 37℃ with 5% CO_2 in Dulbecco's modified Eagle's medium (DMEM) supplemented with 10% horse serum and 5% fetal bovine serum (Gibco-BRL, Gaithersburg, MD). Short hairpin RNAs (shRNA) against rat *Muted* (GenBank RefSeq NM_001107347) were designed by the siRNA target finder (Ambion, Austin, TX). Corresponding DNAs were synthesized and incorporated into the *Bam*HI and *Hin*dIII sites of pSilencer 5.1-H1 Retro (Ambion) vector. The target sequence for *Muted* was 5′-AAGGATCTTGGAGAAATTCAT-3′ and for control was 5′-AATTCTCCGAACGTGTCACGT-3′. These vectors were transfected into PC12 cells using Lipofectamine™ 2000 (Invitrogen, Carlsbad, CA) following the manufacturer's instructions. After 24 hours, the transfected cell clone expressing the vector was selected by 5 µg/ml of puromycin (Invivogen). For the rescue experiment, the *Muted* cDNA (NM_139063.1) was amplified by PCR and cloned in-frame into pEGFP-C2 using the *Xho*I and *Bam*HI sites. Cells were transfected by using the Neon transfection system (Life Technologies, Carlsbad, CA) according to the manufacturer's instruction. Transfected cells were seeded onto poly-D-lysine-coated glass coverslips and then processed for immunostaining 72 hours after transfection.

Chromaffin cells were isolated as previously described (Sørensen et al., 2003) with minimal modifications. Adrenal glands were dissected from 6- to 8-week-old heterozygous *mu*/+ or *mu* mice, placed in filtered Locke's buffer (in mM: 154 NaCl, 5.6 KCl, 5.0 HEPES, 3.6 $NaHCO_3$, and 5.6 glucose, pH 7.4). Fat tissue and adrenal cortex was removed from adrenal medulla under a surgical microscope. The medullae were incubated in 0.2 ml equilibrated (95% O_2:5% CO_2) papain solution (40 units/ml in Locke's buffer; the papain was from Sigma-Aldrich) at 37℃ for 1 hour with gentle shaking. The enzyme solution was discarded and replaced with 500 µl culture medium (DMEM supplemented with 10% fetal calf serum, 100 IU/ml penicillin and 100 µg/ml streptomycin). After washing two times in 500 µl culture medium, the medullae were triturated gently through a 10-µl pipette tip. 50 µl cell suspension was plated on poly-D-lysine-coated glass-bottomed dishes to allow the cells to settle for 30 min at 37℃ before supplementing with 2 ml culture medium. The cells were cultured at 37℃ in 5% CO_2 and used within 3 days.

Immunofluorescence confocal imaging

PC12 cells were plated on poly-D-lysine-coated glass coverslips for 24 hours. Cells were fixed with 4% paraformaldehyde for 20 min at room temperature, permeabilized for 15 min with 0.4% Triton X-100 in PBS, blocked for 30 min with 1% BSA in PBS, then incubated for 16 hours at 4℃ with indicated primary antibodies in PBS containing 1% BSA. Cells were subsequently washed and incubated for 1 hour with a Alexa-Fluor-594-conjugated donkey anti-mouse IgG (1:2000; Invitrogen), Alexa-Fluor-594-conjugated donkey anti-rabbit IgG (1:2000; Invitrogen), Alexa-Fluor-488-conjugated donkey anti-goat IgG (1:2000; Invitrogen), Alexa-Fluor-488-conjugated goat anti-rat IgG (1:2000; Invitrogen) or Alexa-Fluor-488-conjugated donkey anti-rabbit IgG (1:2000; Invitrogen) in PBS containing 1% BSA. Confocal images were acquired using a 100× oil objective with NA 1.40 on a Nikon confocal microscope (ECLIPSE Ti-C2, Japan). Images were obtained using the NIS-Elements AR 3.2 software provided by Nikon. For quantification of the fluorescence intensity, the fluorescence signal was obtained from the entire cell, the nucleus was subtracted and image was analyzed with NIH Image J software.

Electron microscopy

Electron microscopy was carried out as previously described (Chen et al., 2008). Briefly, adrenal glands removed from homozygous *mu* mice and heterozygous *mu*/+ littermates (8 weeks old) were fixed with 3% glutaraldehyde in 0.1 M phosphate buffer (pH 7.4) overnight and were postfixed with 1% OsO_4 for 2 hours at 4℃. Tissue samples were then dehydrated in a graded series of ethanol and were embedded in Epon812. Ultra-thin sections (~60 nm) were collected and stained with uranyl acetate and lead citrate. The sections were examined on a FEI Tecnai 20 electron microscope and analyzed with NIH Image J. At least 100 digital images were taken from randomly selected chromaffin cells of two different animals for both genotypes. Numerical density of the secretory granules was calculated as the number of morphologically identifiable LDCVs per section divided by the chromaffin cell cytoplasmic area. Vesicles with a round membrane and an electron-dense core were included in the diameter analysis. Diameters of vesicles and electron-dense cores were determined by direct measurement. The observer was blind to the genotypes.

The islets from age-matched *mu*/+ and *mu/mu* male mice were fixed in 2% paraformaldehyde and 2.5% glutaraldehyde in 0.1 M phosphate buffer (pH 7.4) overnight and were post-fixed with 1% OsO_4 for 2 hours at 4℃. Tissue samples were then dehydrated in a graded series of acetone and were embedded in Spurr (SPI-Chem, West Chester, PA). Ultra-thin sections (~70 nm) were collected and stained with lead citrate. The sections were examined on an electron microscope (JEM 1400; JEOL, Japan) at 80 kV. Digital images were taken from randomly selected α-cells of two different animals for both genotypes.

Capacitance measurements of chromaffin cells

Whole-cell recordings were performed using an EPC-9 amplifier and Pulse software (HEKA, Lambrecht, Germany). A 800 Hz, 20 mV peak-to-peak sinusoid stimulus was applied about a direct current holding potential of 80 mV. The intracellular solution contained (in mM): Cs-glutamate, 145; NaCl, 8; $MgCl_2$, 1; Mg-ATP, 2; Na_2-GTP, 0.3; and Cs-HEPES, 10 (pH 7.2). The extracellular solution contained (in mM) NaCl, 140; KCl, 2.8; $MgCl_2$, 1; $CaCl_2$, 2; HEPES, 10; and glucose, 2 (pH 7.4). Experiments were performed at room temperature.

Amperometry in adrenal slice

We prepared adrenal medulla slices and performed whole-cell recordings as described previously (Chen et al., 2008) by using an EPC9/2 amplifier and Pulse software (HEKA Elektronik, Lambrecht/Pfalz, Germany). For analysis of the kinetic properties of amperometric spikes, including the half-height duration (HHD), the rise time (RT) and quantal size (Q), only events that were >5 s.d. of the noise were used (Zhou and Misler, 1996). Data analysis was carried out using Igor software (WaveMetrix, USA) with a custom-made macro program (Zhou and Misler, 1996).

Statistics

All values in the text are shown as mean±s.e.m. Student's *t*-test was used to compare means of two groups. Differences of $P<0.05$ were considered statistically significant.

Acknowledgements

We are in debt to Dr. Richard T. Swank for his generous providing of the HPS mutant mice used for this study and for his proofreading of this manuscript. We thank Ms. Lei Sun for her help in making electron microscopy samples and taking electron microscopy images.

Competing interests

The authors declare no competing or financial interests.

Author contributions

W.L., L.C, Z.Z. and Z.H. designed the assays and analyzed the data. W.L. and Z.H. wrote the manuscript. Z.H., Y.F. and J.M. performed the immunostaining, immunoblotting and electron microscopy assays. L.W., X.C., W.D. and Z.H. performed the electrophysiological and amperometric recordings.

Funding

This work was partially supported by grants from the National Natural Science Foundation of China [grant numbers 31230046; 91332116]; the Ministry of Science and Technology of China [grant numbers 2013CB530605, 2014CB942803]; and the Chinese Academy of Sciences [grant number KJZD-EW-L08].

Supplementary material

Supplementary material available online at
http://jcs.biologists.org/lookup/suppl/doi:10.1242/jcs.161414/-/DC1

References

Angers, C. G. and Merz, A. J. (2009). HOPS interacts with Apl5 at the vacuole membrane and is required for consumption of AP-3 transport vesicles. *Mol. Biol. Cell* **20**, 4563-4574.

Arvan, P. and Castle, D. (1998). Sorting and storage during secretory granule biogenesis: looking backward and looking forward. *Biochem. J.* **332**, 593-610.

Asensio, C. S., Sirkis, D. W. and Edwards, R. H. (2010). RNAi screen identifies a role for adaptor protein AP-3 in sorting to the regulated secretory pathway. *J. Cell Biol.* **191**, 1173-1187.

Asensio, C. S., Sirkis, D. W., Maas, J. W., Jr, Egami, K., To, T. L., Brodsky, F. M., Shu, X., Cheng, Y. and Edwards, R. H. (2013). Self-assembly of VPS41 promotes sorting required for biogenesis of the regulated secretory pathway. *Dev. Cell* **27**, 425-437.

Cai, Q., Lu, L., Tian, J. H., Zhu, Y. B., Qiao, H. and Sheng, Z. H. (2010). Snapin-regulated late endosomal transport is critical for efficient autophagy-lysosomal function in neurons. *Neuron* **68**, 73-86.

Chen, X. W., Feng, Y. Q., Hao, C. J., Guo, X. L., He, X., Zhou, Z. Y., Guo, N., Huang, H. P., Xiong, W., Zheng, H. et al. (2008). DTNBP1, a schizophrenia susceptibility gene, affects kinetics of transmitter release. *J. Cell Biol.* **181**, 791-801.

Ciciotte, S. L., Gwynn, B., Moriyama, K., Huizing, M., Gahl, W. A., Bonifacino, J. S. and Peters, L. L. (2003). Cappuccino, a mouse model of Hermansky-Pudlak syndrome, encodes a novel protein that is part of the pallidin-muted complex (BLOC-1). *Blood* **101**, 4402-4407.

Duncan, R. R., Greaves, J., Wiegand, U. K., Matskevich, I., Bodammer, G., Apps, D. K., Shipston, M. J. and Chow, R. H. (2003). Functional and spatial segregation of secretory vesicle pools according to vesicle age. *Nature* **422**, 176-180.

Falcón-Pérez, J. M., Starcevic, M., Gautam, R. and Dell'Angelica, E. C. (2002). BLOC-1, a novel complex containing the pallidin and muted proteins involved in the biogenesis of melanosomes and platelet-dense granules. *J. Biol. Chem.* **277**, 28191-28199.

Feng, Y. Q., Zhou, Z. Y., He, X., Wang, H., Guo, X. L., Hao, C. J., Guo, Y., Zhen, X. C. and Li, W. (2008). Dysbindin deficiency in sandy mice causes reduction of snapin and displays behaviors related to schizophrenia. *Schizophr. Res.* **106**, 218-228.

Gerrish, A., Williams, H., Moskvina, V., Owen, M. J., O'Donovan, M. C. and Williams, N. M. (2009). An examination of MUTED as a schizophrenia susceptibility gene. *Schizophr. Res.* **107**, 110-111.

Ghiani, C. A. and Dell'Angelica, E. C. (2011). Dysbindin-containing complexes and their proposed functions in brain: from zero to (too) many in a decade. *ASN Neuro* **3**, e00058.

Grabner, C. P., Price, S. D., Lysakowski, A. and Fox, A. P. (2005). Mouse chromaffin cells have two populations of dense core vesicles. *J. Neurophysiol.* **94**, 2093-2104.

Grabner, C. P., Price, S. D., Lysakowski, A., Cahill, A. L. and Fox, A. P. (2006). Regulation of large dense-core vesicle volume and neurotransmitter content mediated by adaptor protein 3. *Proc. Natl. Acad. Sci. USA* **103**, 10035-10040.

Gwynn, B., Martina, J. A., Bonifacino, J. S., Sviderskaya, E. V., Lamoreux, M. L., Bennett, D. C., Moriyama, K., Huizing, M., Helip-Wooley, A., Gahl, W. A. et al. (2004). Reduced pigmentation (rp), a mouse model of Hermansky-Pudlak syndrome, encodes a novel component of the BLOC-1 complex. *Blood* **104**, 3181-3189.

Hayes, M. J., Bryon, K., Satkurunathan, J. and Levine, T. P. (2011). Yeast homologues of three BLOC-1 subunits highlight KxDL proteins as conserved interactors of BLOC-1. *Traffic* **12**, 260-268.

John Peter, A. T., Lachmann, J., Rana, M., Bunge, M., Cabrera, M. and Ungermann, C. (2013). The BLOC-1 complex promotes endosomal maturation by recruiting the Rab5 GTPase-activating protein Msb3. *J. Cell Biol.* **201**, 97-111.

Kim, T., Tao-Cheng, J. H., Eiden, L. E. and Loh, Y. P. (2001). Chromogranin A, an ''on/off'' switch controlling dense-core secretory granule biogenesis. *Cell* **106**, 499-509.

Kim, T., Gondré-Lewis, M. C., Arnaoutova, I. and Loh, Y. P. (2006). Dense-core secretory granule biogenesis. *Physiology (Bethesda)* **21**, 124-133.

Koshimizu, H., Kim, T., Cawley, N. X. and Loh, Y. P. (2010). Chromogranin A: a new proposal for trafficking, processing and induction of granule biogenesis. *Regul. Pept.* **160**, 153-159.

Li, W., Zhang, Q., Oiso, N., Novak, E. K., Gautam, R., O'Brien, E. P., Tinsley, C. L., Blake, D. J., Spritz, R. A., Copeland, N. G. et al. (2003). Hermansky-Pudlak syndrome type 7 (HPS-7) results from mutant dysbindin, a member of the biogenesis of lysosome-related organelles complex 1 (BLOC-1). *Nat. Genet.* **35**, 84-89.

Li, W., Rusiniak, M. E., Chintala, S., Gautam, R., Novak, E. K. and Swank, R. T. (2004). Murine Hermansky-Pudlak syndrome genes: regulators of lysosome-related organelles. *BioEssays* **26**, 616-628.

Li, W., Feng, Y., Hao, C., Guo, X., Cui, Y., He, M. and He, X. (2007). The BLOC interactomes form a network in endosomal transport. *J. Genet. Genomics* **34**, 669-682.

Mahapatra, N. R., O'Connor, D. T., Vaingankar, S. M., Hikim, A. P., Mahata, M., Ray, S., Staite, E., Wu, H., Gu, Y., Dalton, N. et al. (2005). Hypertension from targeted ablation of chromogranin A can be rescued by the human ortholog. *J. Clin. Invest.* **115**, 1942-1952.

Morris, D. W., Murphy, K., Kenny, N., Purcell, S. M., McGhee, K. A., Schwaiger, S., Nangle, J. M., Donohoe, G., Clarke, S., Scully, P. et al. (2008). Dysbindin (DTNBP1) and the biogenesis of lysosome-related organelles complex 1 (BLOC-1): main and epistatic gene effects are potential contributors to schizophrenia susceptibility. *Biol. Psychiatry* **63**, 24-31.

Orci, L., Ravazzola, M., Amherdt, M., Louvard, D. and Perrelet, A. (1985a). Clathrin-immunoreactive sites in the Golgi apparatus are concentrated at the trans pole in polypeptide hormone-secreting cells. *Proc. Natl. Acad. Sci. USA* **82**, 5385-5389.

Orci, L., Ravazzola, M., Amherdt, M., Madsen, O., Vassalli, J. D. and Perrelet, A. (1985b). Direct identification of prohormone conversion site in insulin-secreting cells. *Cell* **42**, 671-681.

Pan, P. Y., Tian, J. H. and Sheng, Z. H. (2009). Snapin facilitates the synchronization of synaptic vesicle fusion. *Neuron* **61**, 412-424.

Portela-Gomes, G. M. and Stridsberg, M. (2001). Selective processing of chromogranin A in the different islet cells in human pancreas. *J. Histochem. Cytochem.* **49**, 483-490.

Rehling, P., Darsow, T., Katzmann, D. J. and Emr, S. D. (1999). Formation of AP-3 transport intermediates requires Vps41 function. *Nat. Cell Biol.* **1**, 346-353.

Scott, I., Webster, B. R., Chan, C. K., Okonkwo, J. U., Han, K. and Sack, M. N. (2014). GCN5-like protein 1 (GCN5L1) controls mitochondrial content through coordinated regulation of mitochondrial biogenesis and mitophagy. *J. Biol. Chem.* **289**, 2864-2872.

Sørensen, J. B., Nagy, G., Varoqueaux, F., Nehring, R. B., Brose, N., Wilson, M. C. and Neher, E. (2003). Differential control of the releasable vesicle pools by SNAP-25 splice variants and SNAP-23. *Cell* **114**, 75-86.

Starcevic, M. and Dell'Angelica, E. C. (2004). Identification of snapin and three novel proteins (BLOS1, BLOS2, and BLOS3/reduced pigmentation) as subunits of biogenesis of lysosome-related organelles complex-1 (BLOC-1). *J. Biol. Chem.* **279**, 28393-28401.

Swank, R. T., Novak, E. K., McGarry, M. P., Rusiniak, M. E. and Feng, L. (1998). Mouse models of Hermansky Pudlak syndrome: a review. *Pigment Cell Res.* **11**, 60-80.

Talbot, K., Ong, W. Y., Blake, D. J., Tang, J., Louneva, N., Carlson, G. C. and Arnold, S. E. (2009). Dysbindin-1 and its protein family with special attention to the potential role of dysbindin-1 in neuronal functions and the pathophysiology of schizophrenia. In *Handbook of Neurochemistry and Molecular Neurobiology: Schizophrenia*, 3rd edn, Vol. 27 (ed. D. Javitt and J. Kantrowitz), pp. 107-241. New York, NY: Springer Science.

Tian, J. H., Wu, Z. X., Unzicker, M., Lu, L., Cai, Q., Li, C., Schirra, C., Matti, U., Stevens, D., Deng, C. et al. (2005). The role of Snapin in neurosecretion: snapin knock-out mice exhibit impaired calcium-dependent exocytosis of large dense-core vesicles in chromaffin cells. *J. Neurosci.* **25**, 10546-10555.

Tooze, J. and Tooze, S. A. (1986). Clathrin-coated vesicular transport of secretory proteins during the formation of ACTH-containing secretory granules in AtT20 cells. *J. Cell Biol.* **103**, 839-850.

Tooze, S. A., Martens, G. J. and Huttner, W. B. (2001). Secretory granule biogenesis: rafting to the SNARE. *Trends Cell Biol.* **11**, 116-122.

Voets, T., Neher, E. and Moser, T. (1999). Mechanisms underlying phasic and sustained secretion in chromaffin cells from mouse adrenal slices. *Neuron* **23**, 607-615.

Walter, A. M., Kurps, J., de Wit, H., Schöning, S., Toft-Bertelsen, T. L., Lauks, J., Ziomkiewicz, I., Weiss, A. N., Schulz, A., Fischer von Mollard, G. et al. (2014). The SNARE protein vti1a functions in dense-core vesicle biogenesis. *EMBO J.* **33**, 1681-1697.

Wang, H., Yuan, Y., Zhang, Z., Yan, H., Feng, Y. and Li, W. (2014). Dysbindin-1C is required for the survival of hilar mossy cells and the maturation of adult newborn neurons in dentate gyrus. *J. Biol. Chem.* **289**, 29060-29072.

Watanabe, T., Uchiyama, Y. and Grube, D. (1991). Topology of chromogranin A and secretogranin II in the rat anterior pituitary: potential marker proteins for distinct secretory pathways in gonadotrophs. *Histochemistry* **96**, 285-293.

Wei, A. H. and Li, W. (2013). Hermansky-Pudlak syndrome: pigmentary and non-pigmentary defects and their pathogenesis. *Pigment Cell Melanoma Res.* **26**, 176-192.

Wilkin, M., Tongngok, P., Gensch, N., Clemence, S., Motoki, M., Yamada, K., Hori, K., Taniguchi-Kanai, M., Franklin, E., Matsuno, K. et al. (2008). Drosophila HOPS and AP-3 complex genes are required for a Deltex-regulated activation of notch in the endosomal trafficking pathway. *Dev. Cell* **15**, 762-772.

Yang, Q., He, X., Yang, L., Zhou, Z., Cullinane, A. R., Wei, A., Zhang, Z., Hao, Z., Zhang, A., He, M. et al. (2012). The BLOS1-interacting protein KXD1 is involved in the biogenesis of lysosome-related organelles. *Traffic* **13**, 1160-1169.

Yu, Y., Wang, L., Jiu, Y., Zhan, Y., Liu, L., Xia, Z., Song, E., Xu, P. and Xu, T. (2011). HID-1 is a novel player in the regulation of neuropeptide sorting. *Biochem. J.* **434**, 383-390.

Yuan, Y., Wang, H., Wei, Z. and Li, W. (2015). Impaired autophagy in hilar mossy cells of the dentate gyrus and its implication in schizophrenia. *J. Genet. Genomics* **42**, 1-8.

Zhang, Q., Li, W., Novak, E. K., Karim, A., Mishra, V. S., Kingsmore, S. F., Roe, B. A., Suzuki, T. and Swank, R. T. (2002). The gene for the muted (mu) mouse, a model for Hermansky-Pudlak syndrome, defines a novel protein which regulates vesicle trafficking. *Hum. Mol. Genet.* **11**, 697-706.

Zhang, A., He, X., Zhang, L., Yang, L., Woodman, P. and Li, W. (2014). Biogenesis of lysosome-related organelles complex-1 subunit 1 (BLOS1) interacts with sorting nexin 2 and the endosomal sorting complex required for transport-I (ESCRT-I) component TSG101 to mediate the sorting of epidermal growth factor receptor into endosomal compartments. *J. Biol. Chem.* **289**, 29180-29194.

Zhou, Z. and Misler, S. (1996). Amperometric detection of quantal secretion from patch-clamped rat pancreatic beta-cells. *J. Biol. Chem.* **271**, 270-277.

Journal of Cell Science